

PHOTOPHORETIC STRUCTURING OF CIRCUMSTELLAR DUST DISKS

TAKU TAKEUCHI¹ AND OLIVER KRAUSS²

Accepted by the Astrophysical Journal

ABSTRACT

We study dust accumulation by photophoresis in optically thin gas disks. Using formulae of the photophoretic force that are applicable for the free molecular regime and for the slip-flow regime, we calculate dust accumulation distances as a function of the particle size. It is found that photophoresis pushes particles (smaller than 10 μm) outward. For a Sun-like star, these particles are transported to 0.1 – 100 AU, depending on the particle size, and forms an inner disk. Radiation pressure pushes out small particles ($\lesssim 1 \text{ mm}$) further and forms an extended outer disk. Consequently, an inner hole opens inside $\sim 0.1 \text{ AU}$. The radius of the inner hole is determined by the condition that the mean free path of the gas molecules equals the maximum size of the particles that photophoresis effectively works on (100 μm – 10 cm, depending on the dust property). The dust disk structure formed by photophoresis can be distinguished from the structure of gas-free dust disk models, because the particle sizes of the outer disks are larger, and the inner hole radius depends on the gas density.

Subject headings: circumstellar matter — planetary systems: formation — solar system: formation

1. INTRODUCTION

Protoplanetary disks are composed of gas and dust. At initial stages of their evolution, the gas of protoplanetary disks is as massive as $10^{-3} - 10^{-1} M_{\odot}$ (Greaves 2004), and small dust particles are mixed with the gas, making the disks optically thick at optical wavelengths. As the dust particles grow, the number of small particles reduces, and at a certain stage, the disks become optically thin (Tanaka et al. 2005; Dullemond & Dominik 2005). The amount of gas also decreases, as the gas dissipates (e.g., Hartmann et al. 1998; Clarke et al. 2001; Takeuchi et al. 2005; Alexander et al. 2006a,b). At late stages of the disk evolution, the disks become gas-free dust disks, which are observed as Vega-type disks. During the transition from protoplanetary disks to Vega-type disks, there may be a stage where the disks are optically thin, but their gas component still remains. An example is HD 141569A, which is a 5 Myr Herbig Be star (Weinberger et al. 2000) and has an optically thin dust disk (Augereau et al. 1999; Weinberger et al. 1999; Fisher et al. 2000; Mouillet et al. 2001; Marsh et al. 2002; Clampin et al. 2003). The gas component of this system has been observed (Zuckerman 1995; Dent et al. 2005; Goto et al. 2006) and its amount is estimated to be $\lesssim 60 M_{\oplus}$ (Ardila et al. 2005).

Dynamics of dust particles in optically thin gas disks is of interest in order to investigate the structure of transitional disks. Krauss & Wurm (2005) considered the motion of dust particles in a gas disk that is optically thin at optical wavelengths. A dust particle receives stellar radiation directly, and the radiation pressure pushes the particle outward. In addition to radiation pressure, interaction between the particle and the surrounding gas molecules induces photophoresis, which also pushes the particle outward (see also Wurm & Krauss 2006; Krauss

et al. 2007). When these outward accelerations act with the gas drag on the particle, the particle drifts outward (Takeuchi & Artymowicz 2001). In the outer part of the disk ($\gtrsim 10 \text{ AU}$), where the mean free path of the gas molecules is larger than the particle size (of $\lesssim 1 \text{ m}$), the photophoretic force is proportional to the gas density. When a particle moves outward to the point where the gas density is no longer high enough to induce a strong photophoretic force, the particle's outward motion stops. Consequently, the dust particles pile-up at a certain distance from the star that is determined by the density profile of the gas disk. In a gas disk with mass $\sim 0.01 M_{\odot}$, particles of 100 μm to 10 cm pile-up at several tens of AU. This spontaneous ring formation is a characteristic feature that is caused by photophoresis in a gaseous dust disk.

Krauss et al. (2007) have demonstrated that photophoretic dust motion may be the key process for the transition from optically thick protoplanetary disks to optically thin circumstellar disks with ring-like dust distributions via the stage of transitional disks with an inner hole and a more or less sharp transition to the outer disk that is continuously pushed outward. This outward dust migration can also explain the presence of material formed close to the sun like chondrules and CAIs in asteroids of the main asteroid belt (Wurm & Krauss 2006) or high temperature crystalline silicates in comets from the Kuiper belt (Petit et al. 2006; Brownlee et al. 2006; Mousis et al. 2007).

In this paper, we seek to investigate other characteristic structures formed by photophoresis, especially in the inner part of the disk, but at a stage when most of the dust has already been built into larger bodies. Krauss & Wurm (2005) focus on the dust dynamics in the outer part of the disk ($\gtrsim 10 \text{ AU}$) and use a formula for the photophoretic force that is relevant for low gas densities. In order to investigate the structure of the whole disk, we use a photophoresis formula that can be applied to the whole range of gas densities. Details of the formula for the photophoretic force adopted here are described in §2.

¹ Department of Earth and Planetary Sciences, Kobe University, Kobe 657-8501, Japan; taku@kobe-u.ac.jp

² Institut für Planetologie, Westfälische Wilhelms-Universität Münster, Wilhelm-Klemm-Str. 10, 48149 Münster, Germany; okrauss@uni-muenster.de

Using this formula, we find that photophoresis does not induce dust pile-up at the innermost region of the disk ($\lesssim 0.1$ AU), leading to the formation of an inner hole (see §3). At the inner part of the gas disk, the gas density may be too high that the gas disk itself is no longer optically thin to the stellar radiation, and thus any radiation effects on the dust such as radiation pressure and photophoresis do not work at all. In order to investigate whether photophoresis still works at the inner disk, in §4, we calculate the optical depth of the disk due to Rayleigh scattering of the hydrogen molecules. In §5.1, the thermal relaxation time of dust particles is estimated and is compared to the rotation periods induced by gas turbulence and by photophoresis. In §5.2, we discuss what are the characteristic features that photophoresis forms in dust disks, and what are the observable differences from the gas-free dust disk structures. In Appendix A, a simple calculation deriving the photophoretic force is described.

2. RADIAL DRIFT OF DUST PARTICLES

2.1. Forces Acting on Dust Particles

We consider the motion of a dust particle that resides in a gas disk around a star. The gas disk is assumed to be optically thin in the radial direction. This means that the dust particle directly receives the radiation of the central star. The stellar radiation that is absorbed or scattered by the particle pushes it outward. This outward force, which is called radiation pressure (Burns et al. 1979), is given by

$$F_{\text{rad}} = \frac{\pi a^2 Q_{\text{rad}} I}{c}, \quad (1)$$

where we assume that the particle is spherical and its radius is a , Q_{rad} is the efficiency factor of the radiation pressure and assumed to be unity in this paper, and c is the speed of light. We assume that the particle is on the midplane of the gas disk and the distance from the central star is r . The flux of the stellar radiation at the particle position is

$$I = \frac{L}{4\pi r^2}, \quad (2)$$

where L is the luminosity of the central star. Poynting-Robertson (PR) drag can be neglected comparing to gas drag. Even in a gas disk whose mass is as small as several earth mass, gas drag is much stronger than PR drag as discussed below in §3.4 (see also Takeuchi & Artymowicz 2001).

If the particle's hemisphere facing the central star becomes hotter than the opposite hemisphere, the particle receives the photophoretic force in addition to the radiation pressure. Because, in general, the particle rotates with a certain speed, a considerable temperature gradient appears only if the thermal relaxation time of the particle is much smaller than the rotation period (see discussion in §5.1 below), or if the rotation axis is aligned in the direction of the light source (Krauss et al. 2007). In this paper, we assume that the effect of the particle rotation can be neglected. In this case, the photophoretic force is directed in the radial direction and its value can be analytically calculated. In Appendix A, we describe estimate of the photophoretic force derived by a simple

model of cylindrical dust particles, but we use the rigorous formulae that have been derived in the literature in the following discussion.

We consider a spherical dust particle of radius a . The mean temperature T_d of the particle is in general different from the surrounding gas temperature T_g . In this paper, we simply assume that $T_d = T_g$. The temperature gradient inside the particle is assumed to be small, and then the photophoretic force is calculated by solving linearized perturbation equation of the temperature. In Appendix A, we discuss the cases where the above assumptions are not valid.

If the particle radius, a , is much smaller than the mean free path of the surrounding gas molecules, l , i.e., the Knudsen number $\text{Kn} \equiv l/a \gg 1$, then the photophoretic force is calculated with the free molecular approximation (Hidy & Brock 1967; Mackowski 1989; Beresnev et al. 1993) and is given by

$$F_{\text{ph,f}} = \frac{\pi \alpha J_1 P I a^2}{3[k_d T_d / a + 4\epsilon \sigma_{\text{SB}} T_d^4 + \alpha P v_T / 2]}, \quad (3)$$

where P is the gas pressure, k_d is the thermal conductivity inside the particle, ϵ is the particle's emissivity of thermal radiation and assumed to be unity, σ_{SB} is the Stefan-Boltzmann constant, and v_T is the mean thermal velocity of the gas molecules. The asymmetry parameter J_1 represents how effectively the incident starlight induces a temperature gradient inside the particle. If the incident light is perfectly absorbed at the particle surface, the asymmetry parameter J_1 has the maximum value 0.5, and it becomes smaller as the temperature gradient becomes smaller. The gas molecules that hit the particle are assumed to leave the particle with the Maxwell velocity distribution of the local surface temperature of the particle (i.e., the accommodation factor $\alpha = 1$). In many cases, the denominator of equation (3) is dominated by the first or second terms, i.e., the temperature gradient in the particle is determined by the internal thermal conduction or by the radiative cooling, rather than by the thermal conduction to the gas. In this case, the photophoretic force is approximated by

$$F_{\text{ph,f}} \approx \frac{\pi \alpha J_1 k_B I a^2}{3\sqrt{2} \sigma_{\text{mol}} k_d (1 + 4\epsilon \sigma_{\text{SB}} T_d^3 a / k_d)} \text{Kn}^{-1}, \quad (4)$$

where we used $P = n_g k_B T_g$ and $l = 1/(\sqrt{2} n_g \sigma_{\text{mol}})$, and n_g is the number density of the gas molecules, k_B is the Boltzmann constant, and σ_{mol} is the collisional cross section of the gas molecules. In the free molecular regime, the photophoretic force is inversely proportional to the gas mean free path and proportional then to the gas density.

If the particle size, a , is much larger than the mean free path of the gas molecules, l , i.e., the Knudsen number $\text{Kn} \ll 1$, then the photophoretic force is calculated with the slip-flow approximation (Mackowski 1989). Mackowski (1989) calculated the photophoretic force assuming that the thermal radiation from the particle surface can be neglected. When the thermal radiation is taken into account, his formula is modified to (see Appendix B for the derivation)

$$F_{\text{ph,s}} = \frac{4\sqrt{2} C_s J_1 k_B I a^2}{k_d \sigma_{\text{mol}} d} \text{Kn}, \quad (5)$$

where

$$d = (1+3C_m\text{Kn}) \left[\left(\frac{4\varepsilon\sigma_{\text{SB}}T_d^3 a}{k_d} + 1 \right) (1 + 2C_t\text{Kn}) + 2 \frac{k_g}{k_d} \right], \quad (6)$$

and C_s , C_m , and C_t are the coefficients for the jump conditions at the surface and are of order of unity. We adopt the values of $C_s = 1.17$, $C_m = 1.14$, and $C_t = 2.18$ (Mackowski 1989). The thermal conductivity of the gas is

$$k_g = \frac{15}{8} l v_T n_g k_B, \quad (7)$$

where we set the Prandtl number to be $2/3$. When d is approximated by unity, i.e., $\text{Kn} \ll 1$, $4\varepsilon\sigma_{\text{SB}}T_d^3 a/k_d \ll 1$, and $k_g/k_d \ll 1$, the photophoretic force is proportional to the gas mean free path.

To connect the above two regimes, we introduce the following formula

$$F_{\text{ph}} = \frac{\text{Kn}^2 F_{\text{ph},f} + F_{\text{ph},s}}{1 + \text{Kn}^2}. \quad (8)$$

In the limit of $\text{Kn} \ll 1$, F_{ph} approaches $F_{\text{ph},s}$, and in the other limit ($\text{Kn} \gg 1$), it approaches $F_{\text{ph},f}$.

If the particle rotation cannot be neglected, there are two effects we must consider. First, the temperature gradient in the particle becomes smaller as the particle rotates faster. This effectively reduces the asymmetry factor J_1 . In the limit of rapid rotation, the asymmetry factor J_1 approaches zero. Second, the temperature gradient generally does not coincide with the direction of the light source, i.e., the radial direction. The photophoretic force has a component in the azimuthal direction, and can give or take away angular momentum of the particle, depending on the orientation of the rotation. The particle drifts outward or inward, and the direction of the drift reverses when the orientation of the rotation changes. This is similar to the Yarkovsky effect acting on asteroids (Bottke et al. 2002), although, in the case of photophoresis, the agents of momentum transfer are the gas molecules and not emitted photons. The particle radial drift due to this effect is stochastic, if the variation in the rotational orientation occurs frequently before the particle travels a large distance in the radial direction. Though the study of photophoretic Yarkovsky effect is important, we leave this for future investigations, and in this paper we assume that the photophoretic force is always directed to the radial direction.

For further discussion, it is convenient to normalize the radiative forces given above by the gravitational force

$$F_{G,d} = -\frac{GMm_d}{r^2}, \quad (9)$$

where G is the gravitational constant, M is the mass of the central star, and m_d is the mass of the particle. We introduce a normalization factor

$$\beta = \beta_{\text{rad}} + \beta_{\text{ph}}, \quad (10)$$

where

$$\beta_{\text{rad}} = \left| \frac{F_{\text{rad}}}{F_{G,d}} \right| = \frac{3Q_{\text{rad}}L}{16\pi GMc\rho_d a}, \quad (11)$$

and

$$\beta_{\text{ph}} = \left| \frac{F_{\text{ph}}}{F_{G,d}} \right|. \quad (12)$$

In the free molecular regime ($\text{Kn} \gg 1$),

$$\beta_{\text{ph}} = \frac{\alpha J_1 k_B L}{16\sqrt{2}\pi GM\sigma_{\text{mol}}k_d\rho_d l(1 + 4\varepsilon\sigma_{\text{SB}}T_d^3 a/k_d)}. \quad (13)$$

At large distances from the star, the dust temperature is so low that $4\varepsilon\sigma_{\text{SB}}T_d^3 a/k_d \ll 1$, and that β_{ph} is independent of the particle radius a .

Next we consider the forces acting on the gas. The gravity acting on a unit volume of the gas is

$$F_{G,g} = -\frac{GM\rho_g}{r^2}, \quad (14)$$

where ρ_g is the mass density of the gas. The pressure gradient force on a unit volume is

$$F_{\nabla P} = -\frac{\partial P}{\partial r}. \quad (15)$$

We introduce a normalization factor η in a similar way to the dust particle,

$$\eta = \left| \frac{F_{\nabla P}}{F_{G,g}} \right|. \quad (16)$$

2.2. Gas Disk Models and Dust Parameters

For simplicity, we assume that the gas disk has a power-law profile of the temperature, T_g , in the radial direction r , and is isothermal in the vertical direction z , i.e., it is written as

$$T_g(r) = T_{g,0} r_{\text{AU}}^{-q}, \quad (17)$$

where the subscript “0” denotes quantities at 1 AU, and the non-dimensional quantity r_{AU} is the radius in AU. The gas density, ρ_g , is also assumed to have a power-law profile in r and be in a hydrostatic equilibrium in z , i.e.,

$$\rho_g(r, z) = \rho_{g,0} r_{\text{AU}}^{-p_m} \exp\left(-\frac{z^2}{2h_g^2}\right), \quad (18)$$

where the disk scale height is $\sqrt{2}h_g$. The isothermal sound speed of the disk is $c_s = c_0 r_{\text{AU}}^{-q/2}$, and h_g is written by

$$h_g(r) = \frac{c_s}{\Omega_K} = h_0 r_{\text{AU}}^{(-q+3)/2}, \quad (19)$$

where $\Omega_K = (GM/r^3)^{1/2}$ is the Keplerian angular frequency at the disk midplane. The gas surface density is

$$\Sigma_g(r) = \int_{-\infty}^{+\infty} \rho_g dz = \sqrt{2\pi}\rho_0 h_0 r_{\text{AU}}^{-p}, \quad (20)$$

where $p = p_m + (q-3)/2$. We adopt the following fiducial parameters for the central star and the gas temperature profile: $M = 1 M_{\odot}$, $L = 1 L_{\odot}$, $T_{g,0} = 278$ K, $h_0 = 3.33 \times 10^{-2}$ AU, and $q = \frac{1}{2}$. The mean mass of the gas molecules is $2.34m_{\text{H}}$, where m_{H} is the mass of a hydrogen atom (Nakagawa et al. 1986). The collisional cross section of the gas molecules is $\sigma_{\text{mol}} = 2 \times 10^{-15}$ cm² (p. 228 in Chapman & Cowling 1970).

We consider disks in which most of small dust grains have been removed and consequently the disks have become optically thin even in the radial direction. The dust opacity in optical wavelength arises mainly from

particles smaller than $10 \mu\text{m}$ (see Fig. 4 of Miyake & Nakagawa 1993). In order for the disk to be optically thin, the column density of small grains ($\lesssim 10 \mu\text{m}$) from the star must be smaller than $10^{-3} \text{ g cm}^{-2}$. Removal of dust grains probably occurs through coagulation of the grains into planetesimals (Weidenschilling & Cuzzi 1993; Tanaka et al. 2005; Dullemond & Dominik 2005; Nomura & Nakagawa 2006). In such disks, the amount of the gas component has likely also reduced. Actually most Vega-type stars do not have detectable gas components (Liseau & Artymowicz 1998; Greaves et al 2000; Coulson et al. 2004; Chen & Kamp 2004), and only a few objects have gas as massive as several tens earth masses. For example, HD 141569A has a gas mass of $\lesssim 60M_{\oplus}$ (Zuckerman et al. 1995; Ardila et al. 2005). Therefore, in model A, we consider a disk in which the amount of the gas inside 100 AU is $M_g = 2.4 \times 10^{-5} M_{\odot} = 7.9M_{\oplus}$. (The model disk extends over 100 AU. We specify the disk mass as the mass inside 100 AU.) We take a surface density profile proposed by Hayashi et al. (1985) in which the power-law index is $p = 1.5$. The gas surface density is $\Sigma_g = 1.7 r_{\text{AU}}^{-1.5} \text{ g cm}^{-2}$. In addition to model A, we also consider a more massive disk to investigate a case in which the disk opacity due to the dust has been significantly reduced before considerable gas dissipation occurs. In model B, the gas amount inside 100 AU is $M_g = 1.2 \times 10^{-2} M_{\odot}$. Further, we assume the density profile is more gradual than model A and $p = 0.5$. This gentle slope of the density profile assures that the gas density in the innermost part of the disk (say ~ 0.1 AU) does not become so high that the Rayleigh scattering by molecular hydrogen makes the gas disk itself become optically thick to the starlight (see §4.1 below). The gas surface density in model B is $\Sigma_g = 25 r_{\text{AU}}^{-0.5} \text{ g cm}^{-2}$.

For dust particles, we use the following fiducial parameters: The thermal conductivity $k_d = 10^2 \text{ erg s}^{-1} \text{ cm}^{-1} \text{ K}^{-1}$, the particle bulk density $\rho_d = 1 \text{ g cm}^{-3}$, and the asymmetry factor $J_1 = 0.5$, the emissivity $\varepsilon = 1$, and perfect accommodation of gas molecules $\alpha = 1$. The adopted value of the thermal conductivity is typical for porous aggregates (Presley & Christensen 1997). If the dust particles are more compact, the thermal conductivity can be much higher.

2.3. Radial Motion of Dust Particles

Both the radiation pressure and the photophoretic force direct outward. If the sum of these forces is stronger than the gravity of the central star, i.e., $\beta > 1$, then the particle is not bound to the central star and is ejected from the system. If $\beta < 1$, the particle is bound to the central star, but it feels a net force weaker than the gravity of the central star, and its orbital motion is slower than Keplerian. Assuming the particle's orbit is circular and neglecting any contribution of the gas drag force, the azimuthal velocity of the particle is

$$v_{\theta,d} = (1 - \beta)^{1/2} v_K, \quad (21)$$

where $v_K = (GM/r)^{1/2}$ is the Keplerian velocity. The azimuthal velocity of the gas is also sub-Keplerian because the pressure gradient force usually directs outward, and is given by

$$v_{\theta,g} = (1 - \eta)^{1/2} v_K. \quad (22)$$

Now we consider the effect of the gas drag force acting on a particle that is bound to the central star (i.e., $\beta < 1$). If the particle orbits faster than the surrounding gas ($v_{\theta,d} > v_{\theta,g}$), then the gas drag transfers the angular momentum of the particle to the surrounding gas. Consequently, the particle loses angular momentum and drifts radially to the central star. From equations (21) and (22), it is seen that this inward drift occurs if $\beta < \eta$. On the other hand, if the particle orbits slower than the surrounding gas ($v_{\theta,d} < v_{\theta,g}$, i.e., $\beta > \eta$), then the particle gets angular momentum from the surrounding gas, and drifts radially away from the central star. When the particle happens to be on the orbit in which its azimuthal velocity equals the gas azimuthal velocity, there is no angular momentum transfer by gas drag, and the particle stays on the equilibrium orbit. More detailed discussions including the derivation of the drift velocity were written in Takeuchi & Artymowicz (2001). From their equation (26) for the drift velocity, neglecting the term of the Poynting-Robertson drag, $\beta_c T_s$, gives

$$v_{r,d} = \frac{\beta - \eta}{T_s + T_s^{-1}} v_K, \quad (23)$$

where the non-dimensional stopping time is

$$T_s = \frac{\rho_d a v_K}{\rho_g r v_T}, \quad (24)$$

[the factor 4/3 difference between eq. (10) of Takeuchi & Artymowicz (2001) and eq. (24) comes from the different definition of v_T , see their eq. (6)]

We can know the direction of the particle's radial drift by seeing if β is larger than η or not. Figure 1a shows the ratio β/η against the distance from the central star for model A. If a particle has β larger than η of the surrounding gas, it drifts away from the star, and vice versa. The ratio of radiation pressure to gravity, β_{rad} , which is inversely proportional to the particle radius a , is constant with the distance from the star r (see eq. [11]). On the other hand, as long as the gas mean free path l is larger than the particle radius a (free molecular regime), the photophoretic force is inversely proportional to the Knudsen number Kn (see eq. [4]), and hence decreases with r . Thus, at large distances from the central star, the radiation pressure dominates the photophoretic force, i.e., $\beta \approx \beta_{\text{rad}}$, while at small distances, the photophoretic force dominates and $\beta \approx \beta_{\text{ph}}$. The transition occurs at 1 AU for $10 \mu\text{m}$ particles, 3 AU for $100 \mu\text{m}$ particles, and 7 AU for 1 mm particles. The curves in Figure 1a bend at these distances and the slopes become gentler at larger distances. The slopes of the curves, $d(\beta/\eta)/dr$, are determined only by $d\eta/dr$ at large distances, because β_{rad} is constant with r , and have the same value for differently sized particles. Inside the transition distances, where the photophoretic force dominates, β ($\approx \beta_{\text{ph}}$) increases with decreasing the Knudsen number Kn , or decreasing the distance from the central star. This increase in β continues until the mean free path of the gas molecules l becomes smaller than the particle radius a , i.e., until Kn becomes less than unity. At the innermost part of the disk in which $\text{Kn} < 1$ (slip-flow regime photophoresis), β is proportional to Kn (see eq. [5]) and decreases with decreasing r . The transition from the free molecular regime photophoresis to the slip-flow regime photophoresis oc-

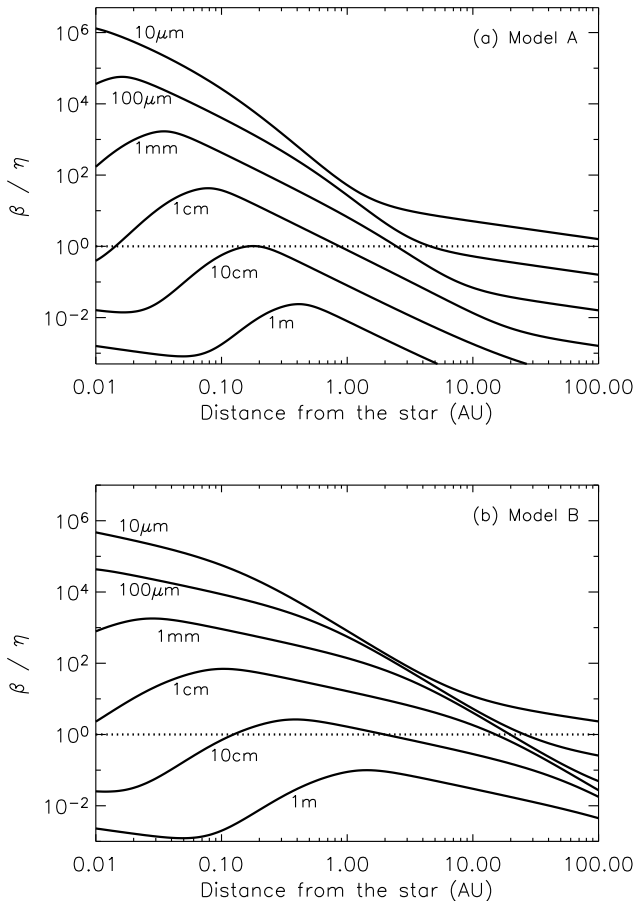


FIG. 1.— Ratio of the normalized outward force on the dust particle, β , with regard to that on the gas, η . The particle size is varied from $10 \mu\text{m}$ to 1 m . The dotted line represents $\beta = \eta$. The particles drift outward if $\beta/\eta > 1$, and drift inward if $\beta/\eta < 1$. (a) For the gas disk model A ($\Sigma_g = 1.7 r_{\text{AU}}^{-1.5} \text{ g cm}^{-2}$, $M_g = 2.4 \times 10^{-5} M_\odot = 7.9 M_\oplus$ inside 100 AU). (b) Model B ($\Sigma_g = 25 r_{\text{AU}}^{-0.5} \text{ g cm}^{-2}$, $M_g = 1.2 \times 10^{-2} M_\odot$).

curs at the distance where $\text{Kn} = 1$, and at this transition distance, β/η has the maximum value. For $100 \mu\text{m}$ particles, β/η has a peak at 0.02 AU , and for larger particles the peak position shifts outward. It is 0.2 AU for 10 cm particles.

It is seen from Figure 1a that particles smaller than 10 cm have a region where β is greater than η . In such a region the particles drift outward. The outward drift of the particles stops at the locations where $\beta = \eta$. At these locations, the particles that drift inward from the outer region also stop. Hence, the particles accumulate at the location where $\beta = \eta$ and $d(\beta/\eta)/dr < 0$, leading to the formation of a dust ring as proposed by Krauss & Wurm (2005). Particle accumulation does not occur at the location where $\beta = \eta$ but $d(\beta/\eta)/dr > 0$, because the particles drift away from such locations. Note that, at the locations where particles accumulate, the Knudsen number Kn is always larger than unity, and thus the photophoretic force is expressed in its form for the free molecular regime. The location of particle accumulation is at 5 AU for $100 \mu\text{m}$ particles, and moves closer to the central star as the particle radius increases. Particles of

10 cm accumulate at 0.2 AU . If the particles are larger than 10 cm , they always drift toward the central star and cannot accumulate anywhere. In summary, particle accumulation occurs if $\beta/\eta > 1$ somewhere in the disk. The accumulation location is specified by the conditions $\beta = \eta$, $d(\beta/\eta)/dr < 0$, and $\text{Kn} > 1$.

For 10 cm and 1 m particles, the curves in Figure 1a again bend at $0.02 - 0.05 \text{ AU}$. Inside these distances, the radiation pressure becomes stronger than the photophoretic force because the Knudsen number is too low. Thus, β keeps constant with r in this region, while η increases, resulting in a decrease in β/η .

A similar result is obtained for model B (Fig. 1b). In this model, particles of all sizes are driven farther outward compared to model A. This is because the gas density is higher in the model B disk, resulting in an increase in β_{ph} . In model B, it is also apparent that $100 \mu\text{m} - 1 \text{ cm}$ particles accumulate in a narrow region of $20 - 30 \text{ AU}$. This pile-up of particles in a narrow ring has been pointed out by Krauss & Wurm (2005). It is the consequence of β_{ph} being independent of the particle radius at large distances (eq. [13]).

Note that accumulation of outward migrating particles to the ring radius do not increase the optical depth to the star. Formation of the dust ring through clearing the inner dust disk does not suppress further evolution by photophoresis. However, after clearing the inner dust, the optical depth of the ring increases as particles from the outer disk accumulate. When the dust ring becomes optically thick, photophoresis is weakened and then the ring shrinks. In this paper, we consider the stage where the dust ring is optically thin.

3. PARTICLE ACCUMULATION RADIUS

As discussed in the above section, particles accumulate at the equilibrium locations where $\beta = \eta$ and $d(\beta/\eta)/dr < 0$. In Figure 2a and 2b the equilibrium distances for model A and model B, respectively, are plotted as functions of the particle radius. The line labeled “fiducial” represents the equilibrium distances calculated with the parameters written in §2.2. The equilibrium distances for other parameters are also plotted. We vary the value of one parameter with keeping the other parameters being the same as the fiducial model. Higher thermal conductivities $k_d = 10^5$ and $10^7 \text{ erg s}^{-1} \text{ cm}^{-1} \text{ K}^{-1}$, a lower bulk density $\rho_d = 0.1 \text{ g cm}^{-3}$, a lower efficiency of photophoresis $J_1 = 0.5 \times 10^{-2}$, and a higher luminosity of the central star $L = 20 L_\odot$ are investigated. We also calculate the case in which photophoresis does not work at all ($J_1 = 0$).

3.1. Dust Concentration and Size Segregation

At the accumulation locations, photophoresis is under the free molecular regime ($\text{Kn} > 1$), and as seen from equation (13), β_{ph} converges to a certain value in the limit of small a . On the other hand, β_{rad} is inversely proportional to a (neglecting the size dependence of Q_{rad}), and thus radiation pressure is more efficient than photophoresis for smaller particles. In the condition $\beta = \eta$ that determines the accumulation location, β is controlled by radiation pressure for small particles, and by photophoresis for large particles. The particle size where the transition from one behavior to the other occurs depends on the parameters that are relevant for

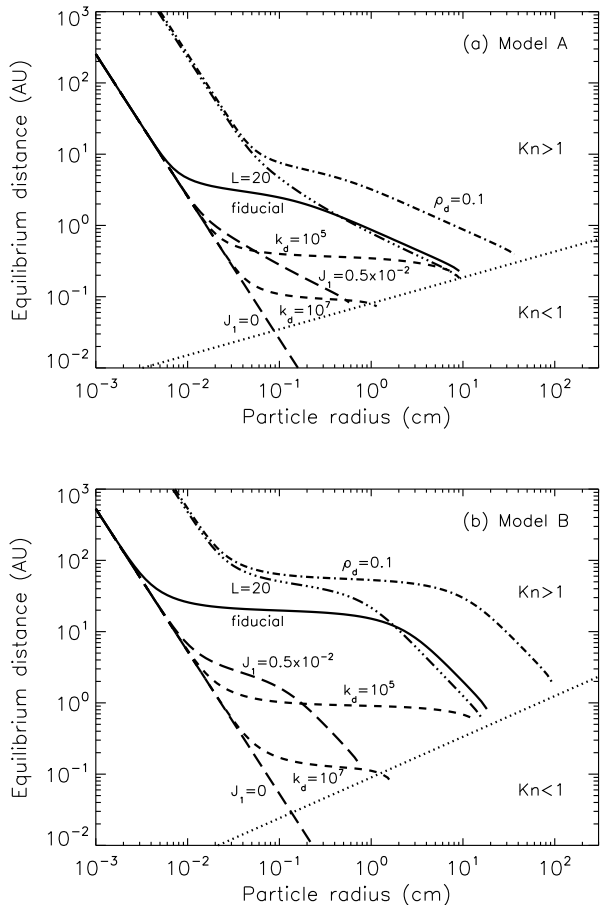


FIG. 2.— Equilibrium distances, where $\beta = \eta$, for the dust particles of the various physical properties: fiducial parameters ($k_d = 10^2 \text{ erg s}^{-1} \text{ cm}^{-1} \text{ K}^{-1}$, $\rho_d = 1 \text{ g cm}^{-3}$, and $J_1 = 0.5$; solid line), higher thermal conductivity ($k_d = 10^5$ and $10^7 \text{ erg s}^{-1} \text{ cm}^{-1} \text{ K}^{-1}$; short dashed lines), smaller efficiency of photophoresis ($J_1 = 0.5 \times 10^{-2}$ and 0 ; long dashed lines), lower bulk density ($\rho_d = 0.1 \text{ g cm}^{-3}$; dot-dashed line), and more luminous star $L = 20L_\odot$ (three dots-dashed line). The dotted line shows the distances where the Knudsen number is unity. Above (below) the dotted line, $\text{Kn} > 1$ ($\text{Kn} < 1$). (a) Model A. (b) Model B.

the strength of the photophoretic force, i.e., k_d and J_1 . This can be seen in Figure 2a where the curves for different parameters depart from the straight line for $J_1 = 0$ at different particle sizes. For the fiducial dust parameters in model A (the solid line in Fig. 2a), the accumulation locations of particles larger than $100 \mu\text{m}$ are controlled by photophoresis, while those of smaller particles are controlled by radiation pressure.

Particles that are subject to photophoresis have the tendency to accumulate in a narrow ring region, provided that all particles have the same physical properties, i.e., they have the same values of ρ_d , k_d , and J_1 . For example, in the fiducial model (the solid line in Fig. 2a), particles of $200 \mu\text{m} - 2 \text{ mm}$ accumulate in a region of $2 - 4 \text{ AU}$, and $300 \mu\text{m} - 10 \text{ cm}$ particles of the higher conductivity $k_d = 10^5 \text{ erg s}^{-1} \text{ cm}^{-1} \text{ K}^{-1}$ accumulate at $0.2 - 0.5 \text{ AU}$. Hence, a significant influence of photophoresis is to condense the particles of a certain size interval. For small particles, this size interval is limited by the increasing influence of radiation pressure. For large particles, the

limit is determined by the increasing importance of thermal emission and conduction to the gas for the thermal relaxation and the approach to $\text{Kn} = 1$. The location of accumulation decreases with increasing thermal conductivity. Thus, particles with different thermal properties can be separated in the disk by this process. While $k_d = 10^2 \text{ erg s}^{-1} \text{ cm}^{-1} \text{ K}^{-1}$ corresponds to very porous dust aggregates, values around $10^5 \text{ erg s}^{-1} \text{ cm}^{-1} \text{ K}^{-1}$ are appropriate for compact rocky or glassy grains and $10^7 \text{ erg s}^{-1} \text{ cm}^{-1} \text{ K}^{-1}$ for purely metallic particles. As discussed by Wurm & Krauss (2006), compact particles like chondrules or CAIs might have been accumulated in the region of the asteroid belt whereas porous dust aggregates were driven farther outwards by photophoresis in the forming solar system (see Fig. 2b for the disk model as massive as the solar nebula).

In actual disks, the properties of particles are probably not homogeneous, but the dust disks are composed of a wide variety of particles. Even particles of the same size therefore spread over a certain range of distances, and the dust ring formed by photophoresis has some extent in the radial direction. We still expect, however, particle concentration in the disk happens to some degree. Even if the parameter range of the particle properties is as wide as that considered in Figure 2a, we clearly see two populations of dust particles. All the particles at distances larger than 10 AU are smaller than 1 mm and do not show any sign of concentration. The dust population inside 10 AU is composed of particles larger than $100 \mu\text{m}$, and is confined in a region between $0.1 - 10 \text{ AU}$. We call this region as an inner disk. These two populations are divided by the condition which of the radiation pressure or the photophoretic force is larger than the other. The population of small particles is subject to radiation pressure, and the other is subject to photophoresis. Hence, the effect of photophoresis is to discriminate large particles from small particles and to confine them to the inner region of the disk.

3.2. Inner Holes

Another significant feature of Figure 2a is that in the region below the dotted line, which represents the area where $\text{Kn} < 1$, there is no equilibrium location where particle accumulation through photophoresis occurs. As discussed in §2.3, particle accumulation by photophoresis always occurs at locations where $\text{Kn} > 1$. If photophoresis does not work ($J_1 = 0$), it is seen in Figure 2a that particles can accumulate even in the region where $\text{Kn} < 1$. This feature will be a possible observational evidence for showing that photophoresis actually occurs in gas disks, though it requires observations of the innermost part of the disk ($r \lesssim 0.1 \text{ AU}$) with a very high spatial resolution. If photophoresis actually works, we would find that an inner hole opens in the dust disk, and that its radius is determined by the condition $\text{Kn} = 1$. If photophoresis does not work, on the other hand, the dust particles would exist even in a region where $\text{Kn} < 1$. An actual dust disk is a mixture of particles of various physical properties. If the dust particles have the range of properties that are considered in Figure 2, the inner radius (that is determined by the particles of $k_d = 10^7 \text{ erg s}^{-1} \text{ cm}^{-1} \text{ K}^{-1}$ or $J_1 = 0.5 \times 10^{-2}$) is $\sim 0.1 \text{ AU}$. This inner radius may be as small as 0.03 AU , if there are considerable numbers of particles on that photophoresis works very weakly (i.e.,

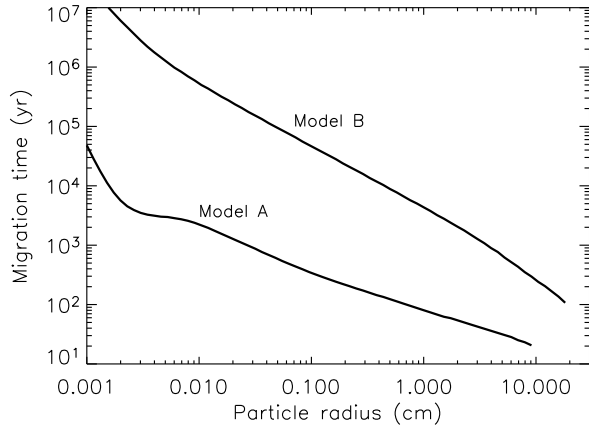


FIG. 3.— Timescales, τ_{mig} , for the dust particles to migrate to the accumulation locations. The dust parameters are the fiducial values.

particles of very small J_1 , but in that case the inner disk clearing is probably suppressed as shown by the $J_1 = 0$ line.)

We stress that the Knudsen number Kn is only a function of the dust particle size a and the mean free path of the gas molecules l . Thus, the inner radii of dust disks do not directly reflect the dust particles' physical properties such as the thermal conductivity k_d , the bulk density ρ_d , and the efficiency of photophoresis J_1 . (The particle size at the inner edge does depend on the particle properties.) The fact that the inner radius of the dust disk is determined only by the particle size considerably helps us when we observationally test the idea of inner hole opening by photophoresis. On the other hand, it is of great importance to have an independent measurement of the local gas density to decide whether the condition $\text{Kn} = 1$ is fulfilled, which might still be a challenging task for modern observational techniques.

3.3. Massive Disks

Figure 2b shows the equilibrium distances with the same parameter combinations as in Figure 2a but for the disk model B. In model B, where the disk mass (inside 100 AU) is 500 times larger than that of model A, 1 mm to 10 cm particles may extend farther from the central star than in model A due to photophoresis (up to ~ 100 AU). The inner radius of the dust disk locates at ~ 0.1 AU (for the particles of $k_d = 10^7 \text{ erg s}^{-1} \text{ cm}^{-1} \text{ K}^{-1}$ or $J_1 = 0.5 \times 10^{-2}$), and is similar to that in model A. This is just because we take such a density distribution for model B that the distances where Kn equals unity for the particle size $a = 1 \text{ mm} - 1 \text{ m}$ do not considerably differ from those in model A. This choice of the density distribution in model B comes from the requirement that the gas disk must be optically thin and we take a marginally optically thin disk (see §4.1 below).

3.4. Timescale of Structure Formation

The timescale for the dust particles to migrate to the accumulation locations is $\tau_{\text{mig}} = |r_{\text{eq}}/v_{r,d}|$, where r_{eq} is the equilibrium distance shown in Figure 2 and $v_{r,d}$ is the radial drift velocity. In equation (23), $\beta \sim \eta$ near the equilibrium distance r_{eq} , and thus the drift velocity $v_{r,d}$

is estimated as $v_{r,d} \sim \eta v_{\text{K}}/(T_s + T_s^{-1})$. The migration timescale is then $\tau_{\text{mig}} \sim (T_s + T_s^{-1})/(\eta \Omega_{\text{K}})$, where the value is calculated at r_{eq} . Figure 3 shows the migration timescales for the fiducial dust parameters of model A and B. For both models, the timescales are shorter than $10^6 - 10^7$ yr, which is the expected age of the transitional disks, except for small particles ($a \lesssim 100 \mu\text{m}$) in model B. Hence, the disk structure and the inner hole are expected to form quickly when the disks have become transparent to the starlight. (In disks more tenuous than model A, photophoresis effectively works only at the dense innermost part of the disk, and thus the dust accumulation location approaches the star. For example, in a disk 10^{-3} times more tenuous than model A, i.e., in a disk of $M_g \sim 10^{-2} M_{\oplus}$, particle accumulation occurs only inside 0.1 AU. The migration timescale for $100 \mu\text{m} - 1 \text{ cm}$ particles at $\lesssim 0.1$ AU is still less than 10^4 yr.)

The migration timescale in Figure 3 is much shorter than the orbital decay time due to Poynting-Robertson (PR) drag. For example, $100 \mu\text{m}$ particles in model A accumulate at 4 AU in $\tau_{\text{mig}} = 2 \times 10^3$ yr. The particles have $\beta_{\text{rad}} = 6 \times 10^{-3}$ and the timescale due to PR drag is $\tau_{\text{PR}} = 400(r/1 \text{ AU})^2 \beta_{\text{rad}}^{-1} \text{ yr} = 10^6 \text{ yr}$ (Burns et al. 1979), and much longer than τ_{mig} . Both in model A and B, it is shown that $\tau_{\text{mig}} \ll \tau_{\text{PR}}$ for any particle size. This means that PR drag is much weaker than gas drag and can be neglected.

4. OPACITY OF THE DISK GAS

In the previous sections, we assumed that the disk is optically thin even in the radial direction and dust particles directly receive the light from the central star. This assumption requires that both the dust and gas opacities of the disk must be small enough. We consider a stage in which most of the dust grains are packed together into planetesimals or larger objects and the disk opacity due to the dust has become negligible. Such a situation has probably been realized in some Vega-type stars. The gas disk also must be transparent, though photophoresis requires a sufficient amount of gas. In this subsection, we discuss whether the gas disk that is dense enough for photophoresis to work is transparent to the starlight.

We assume that the gas disk is mostly composed of hydrogen molecules. Thus, Rayleigh scattering by H_2 is a possible and probably dominant mechanism of light extinction in the disk. In this subsection, we consider the gas opacity due to Rayleigh scattering by H_2 and estimate the maximum gas density at which the gas disk is marginally opaque to the light of the central star. Our estimate gives the lower limit of the gas opacity, because only Rayleigh scattering by H_2 is taken into account, and thus the derived maximum gas density should be considered as an upper limit. A transparent gas disk in which photophoresis works must be less dense than our estimate. If other extinction mechanisms work more effectively than the Rayleigh scattering by H_2 , this upper limit of the density becomes smaller. In §4.2 below, we briefly discuss other extinction mechanisms.

4.1. Rayleigh Scattering by Hydrogen Molecules

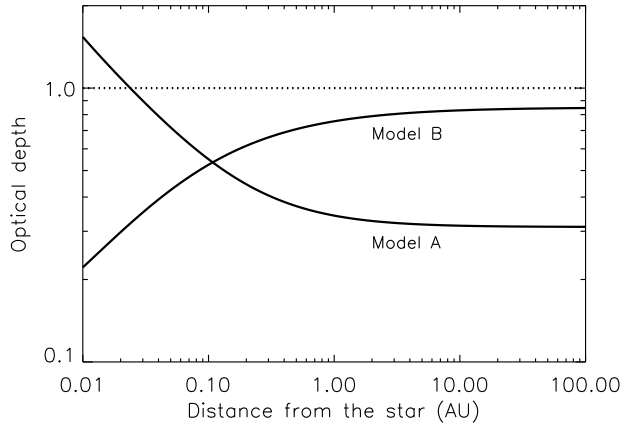


FIG. 4.— Optical depth τ_{H_2} due to Rayleigh scattering of H_2 from the typical point of the star ($0, 0.424R_*$) to the midplane of the disk at $(r, 0)$. The dotted line represents $\tau_{\text{H}_2} = 1$.

The cross section of Rayleigh scattering by H_2 per molecule is

$$\sigma_{\text{H}_2} = 8.4909 \times 10^{-29} \left(\frac{\lambda}{1 \mu\text{m}} \right)^{-4} \text{ cm}^2, \quad (25)$$

where λ is the wavelength of the light (Tsuji 1966). In this subsection, we make an order of magnitude argument, and simply estimate the opacity around the central wavelength of the central star's spectrum, $\lambda = 0.5 \mu\text{m}$. The stellar light source is assumed to be point sources, which are located slightly above and beneath the origin, $z_* = \pm 0.424R_*$, where R_* is the radius of the central star (Hollenbach et al. 1994) and we assume $R_* = 1.0 R_\odot$. The optical depth from the star, $(0, z_*)$, to a dust particle on the midplane, $(r, 0)$, is

$$\tau_{\text{H}_2} = \int \sigma_{\text{H}_2} n_g ds, \quad (26)$$

where n_g is the number density of the gas molecules (we assume all the gas is composed of H_2 for simplicity).

Figure 4 shows the optical depths from the central star as functions of the distance r . In both models A and B, the disks are optically thin (except for $r < 0.03$ AU in model A). Note that the disk mass (inside 100 AU) of model B is 500 times larger than that of model A, but the optical depths from the star are not much different. This is because the opacities of the disks are mainly determined by the density at ~ 0.1 AU and the densities at 0.1 AU in model A and B do not differ much (Fig. 5). The starlight that illuminates a particle located at a distance $r \gg 0.1$ AU gets into the disk at a distance ~ 0.1 AU, because the disk scale height at 0.1 AU is $\sqrt{2}h_g \approx 2 \times 10^{-3}$ AU $\approx 0.4R_* \approx z_*$. Model B has the density profile $\Sigma_g \propto r^{-0.5}$ and most of the gas mass is distributed in the outermost part of the disk, while the density profile of model A is more steep ($\Sigma_g \propto r^{-1.5}$) and the disk mass is more concentrated in the innermost region. Thus, even though the disk mass of model B is 500 times larger than that of model A, the densities at 0.1 AU in model A and B are similar. For particles located much farther than 0.1 AU, the optical depth from the central star does not change with the distance r .

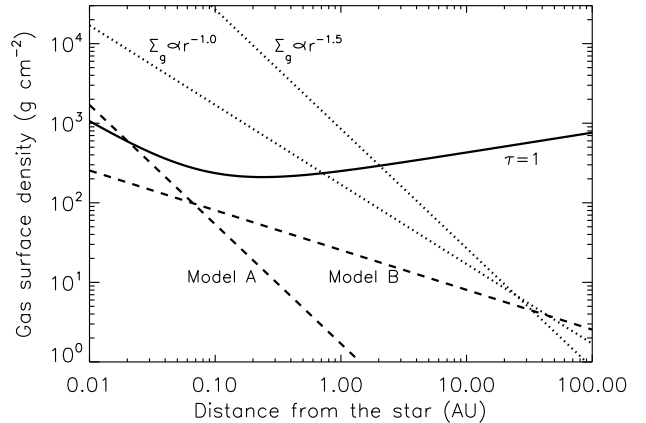


FIG. 5.— Comparison of the density profiles of models A and B (dashed lines) to the maximum gas density required to be optically thin to the central star (solid line). The dotted lines show the density profiles that have the same amount of mass as model B (inside 100 AU) but have different slopes ($\Sigma_g \propto r^{-1.5}$ and $\Sigma_g \propto r^{-1.0}$).

For particles inside ~ 0.1 AU, the location where the starlight enters the disk moves toward the central star as the particle position gets closer to the star. In model A, the optical depth is determined by the gas density at where the starlight enters the disk, which rapidly increases with decreasing the distance r . Consequently, the optical depth increases with decreasing the particle distance. In model B, the concentration of the gas at the innermost part of the disk is moderate. Thus, the decrease in the path length of the starlight (which is approximately proportional to r) dominates the increase in the gas density at where the starlight enters the disk. The optical depth from the star decreases with decreasing the particle distance in model B.

We estimate the maximum gas density of a disk for it to be optically thin. The optical depth to the star from $(r, 0)$ at the disk midplane is estimated as $\tau \approx \sigma_{\text{H}_2} n_g s$, where the number density of hydrogen molecules n_g is estimated at $(r, 0)$, and s is the path length of the starlight. The path length s is the distance between $(r, 0)$ and the point where the starlight enters the disk. The location of the latter point is approximately calculated as the point where the line connecting $(0, 0)$ and $(r, \sqrt{2}h_g)$ crosses the line connecting $(0, z_*)$ and $(r, 0)$. The condition $\tau < 1$ reduces to the condition for the gas surface density $\Sigma_g < \sqrt{2\pi}h_g m_{\text{H}_2} / (\sigma_{\text{H}_2} s)$, where m_{H_2} is the mass of a hydrogen molecule. The solid line in Figure 5 shows the upper limit of the gas surface density for the optical depth to the star to be less than unity. We see that for $r > 0.02$ AU both the surface densities of model A and B (dashed lines) are less than the critical density for $\tau = 1$ (solid line). For comparison, the surface densities of the disks that have the same amount of mass as model B (inside 100 AU) but have different slopes of the density distribution ($\Sigma_g \propto r^{-1.5}$ and $\Sigma_g \propto r^{-1.0}$, dotted lines). It is seen that, if the disk is centrally concentrated, the disk is optically thick at the inner region of the disk.

The condition $\tau < 1$ reduces also to the condition for the mean free path of the gas molecules. The mean free path of the gas must be larger than the value shown as

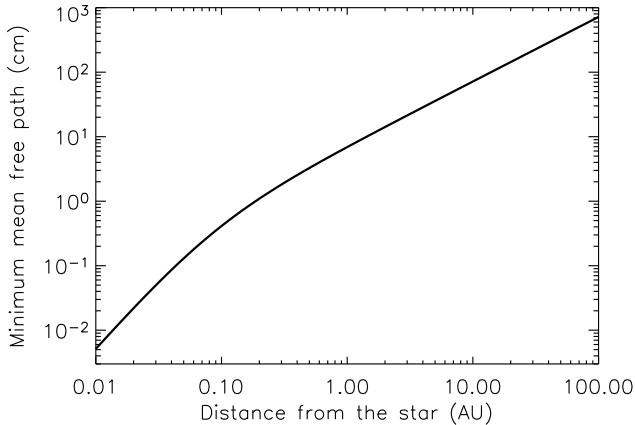


FIG. 6.— Mean free path of the hydrogen molecules in the critical disk where the optical depth to the central star is unity.

the solid line in Figure 6 for the disk to be optically thin. This minimum value is also interpreted as the minimum size of dust particles that compose the inner edge of the dust disk, because the location of the inner edge is determined by the condition $\text{Kn} = 1$. Thus, in order to observationally test whether the inner hole is produced by photophoresis, we have to detect particle accumulation of sizes larger than the value indicated in Figure 6. Suppose that, for example, a dust disk has an inner hole of radius 0.04 AU. If this inner hole is formed by photophoresis, the gas disk at 0.04 AU must be optically thin, and from Figure 6, the mean free path at 0.04 AU must be larger than 1 mm. Because only particles larger than the mean free path can accumulate through photophoresis, the particles at the inner edge must be larger than 1 mm. This minimum particle size becomes larger as the inner radius of the dust disk becomes larger. If the inner radius is 1 AU, the particle size must be larger than 10 cm.

4.2. Other Opacity Sources

1. Bound-free and free-free absorption of negative hydrogen ions — The cross section of bound-free and free-free absorption is proportional to the electron pressure. Thus, this absorption works in environments where the ionization degree is high, and is efficient only at the innermost region of the disk, provided that the disk gas is thermally ionized. In both models A and B, the temperature at 0.02 AU is $T \approx 2000$ K, and the gas pressure is $P_{\text{H}_2} \sim 10^3 \text{ dyn cm}^{-2}$ (the molecular hydrogens dominate the gas pressure). The partial pressures of electrons and of hydrogen atoms are $P_e/P_{\text{H}_2} \sim 10^{-7}$ and $P_{\text{H}}/P_{\text{H}_2} \sim 3 \times 10^{-2}$, respectively (Fig. 1 of Tsuji 1966; the solar abundance is assumed). At the optical wavelength $\lambda = 0.5 \mu\text{m}$, the bound-free absorption dominates the free-free absorption, and the absorption cross section per hydrogen molecule is $\sigma_{\text{H}^-,bf+ff} \sim 10^{-23} P_e P_{\text{H}}/P_{\text{H}_2} \text{ cm}^4 \text{ dyn}^{-1} \sim 3 \times 10^{-29} \text{ cm}^2$, where we used the value of Table 2 of Tsuji (1966). Since the cross section of the bound-free absorption sensitively depends on λ and T , we took the highest value around $\lambda \approx 0.5 \mu\text{m}$ and $T \approx 2000$ K in the Tsuji’s Table as a representative value (we take the value for $\lambda = 0.5 \mu\text{m}$ and $T = 1938$ K). From equation (25), the cross section of Rayleigh

scattering for $\lambda = 0.5 \mu\text{m}$ is $\sigma_{\text{H}_2} = 1.36 \times 10^{-27} \text{ cm}^2$. The cross section of bound-free and free-free absorption is much smaller than that of Rayleigh scattering even at the innermost part ($r = 0.02$ AU) of disk model A and B, and thus can be ignored. (Recall that stellar photons penetrate the disk at ~ 0.1 AU for calculating the optical depth to $r \gg 0.1$ AU.)

2. Free-free absorption of negative hydrogen molecules — This absorption works only at the innermost part of the disks. Thus, we estimate the cross section at 0.02 AU of the model disks, which is $\sigma_{\text{H}_2^-,ff} \sim 10^{-27} P_e \text{ cm}^4 \text{ dyn}^{-1} \sim 10^{-31} \text{ cm}^2$, where we used equation (8) of Tsuji (1966). This value is much smaller than that of Rayleigh scattering, and free-free absorption of negative hydrogen molecules can be ignored.

3. Collision-induced absorption of hydrogen molecules — This absorption works efficiently if the gas pressure is high. The cross section is expressed as $\sigma_{\text{CIA}} = k_{\text{CIA}} n_g/n_{\text{L}}^2$ where k_{CIA} is the opacity in the unit $\text{cm}^{-1} \text{ amagat}^{-2}$ and $n_{\text{L}} = 2.69 \times 10^{19} \text{ cm}^{-3}$ is Loschmidt’s number. We consider the innermost part of the disk. The gas number density at 0.02 AU of model A and B is $n_g \sim 10^{16} \text{ cm}^{-3}$. At the optical wavelength $\lambda = 0.5 \mu\text{m}$, the opacity k_{CIA} due to $\text{H}_2 - \text{H}_2$ and $\text{H}_2 - \text{He}$ collisions is less than $10^{-11} \text{ cm}^{-1} \text{ amagat}^{-2}$ as long as $T < 4000$ K (Fig. 1 and 2 of Borysow et al. 1997). Thus, σ_{CIA} is smaller than 10^{-34} cm^2 , and can be ignored in comparison to Rayleigh scattering.

4. Thomson scattering — The cross section of Thomson scattering per hydrogen molecule is $\sigma_e = 6.65 \times 10^{-25} P_e/P_{\text{H}_2} \text{ cm}^2$. This can be ignored in comparison to Rayleigh scattering, as long as $P_e/P_{\text{H}_2} \ll 10^{-3}$.

5. Molecular absorption bands — At the innermost part of the disk, where the temperature is high enough to vaporize refractory elements from the dust, gas molecules such as TiO and VO contribute to the gas opacity at the optical wavelengths (Tsuji 1971; Alexander & Ferguson 1994; Ferguson et al. 2005). The rotation-vibration lines of such molecules overlap and make a band structure veiling the optical wavelengths. We calculated the gas opacity of model disks A and B due to the molecular absorption bands. In the calculation, we used the code developed by Tsuji (2002) for calculating the opacity of cool stellar atmospheres, and assumed the solar abundance of the gas and dust mixture. At the optical wavelengths ($\lambda \approx 0.5 \mu\text{m}$), absorption by VO becomes stronger than Rayleigh scattering of H_2 for $T > 1300$ K, and absorption by TiO becomes stronger for $T > 1400$ K. Thus, in the disk inside 0.05 AU of models A and B, where the temperature is higher than 1300 K, the gas opacity is dominated by the molecular absorption bands. Our estimate of the gas opacity in §4.1 is not appropriate for the gas inside 0.05 AU. For dust particles at $r \gg 0.1$ AU, the rays from the central star enter the disk at ~ 0.1 AU, where the gas opacity is dominated by Rayleigh scattering, and contribution of the molecular absorption bands can be neglected. Most of refractory elements may be confined in large bodies such as planetesimals and are removed from the gas phase. In such cases, contribution of the molecular absorption bands is reduced.

5.1. Thermal Relaxation and Rotation Times of Dust Particles

As mentioned in §2.1, if particles rotate rapidly, photophoresis does not work. Even if particle rotation is not considerably rapid compared to the thermal relaxation time of the particle, photophoretic Yarkovsky effect may prevent the particle accumulation. Such cases where photophoresis does not work are represented by the model of $J_1 = 0$, where the incident starlight does not cause any temperature gradient in the particles. If photophoresis is suppressed by any reason, particles can reside in the region where $\text{Kn} < 1$ (Fig. 2), and such cases can be observationally distinguished from the disks in which photophoresis clears the dust in the innermost region. Hence, whether particles in gas disks rotate rapidly or not can be observationally investigated by checking whether the dust in the region of $\text{Kn} < 1$ is cleared or not.

In this subsection, we estimate the thermal relaxation time of a dust particle and then compare it to the rotation period induced by gas turbulence or by photophoresis itself. We use a simple model of a cylindrical dust particle described in Appendix A. Consider a cylindrical dust particle with radius a and height $2a$ (see Figure 9). The stellar radiation flux I irradiates the front surface. We suppose that, at the beginning, the temperature inside the particle is homogeneous. This initial (or average) temperature T_d is given by equation (A16), assuming that the incident flux I balances with thermal radiation from the front and back surfaces. (Radiation from the side surface is ignored for simplicity.) The temperature of the front surface increases to the equilibrium value T_f in a thermal relaxation time τ_{th} . During τ_{th} , the incident energy at the front surface conducts for a length δa and forms a skin layer of temperature gradient. During τ_{th} , the temperature at the front surface is approximated as the initial value T_d , and the energy flux inside the skin layer is estimated as $Q_{\text{con}} \approx I - \sigma_{\text{SB}} T_d^4 = I/2$. (We set $\varepsilon = 1$.) When the skin layer depth has grown to δa and the temperature of the front surface converges to T_f , the energy flux is $Q_{\text{con}} \approx k_d(T_f - T_d)/\delta a$. Equating the above two expressions for Q_{con} , the thickness of the temperature gradient layer is

$$\delta a = \frac{2k_d T_d \Delta}{I}, \quad (27)$$

where $\Delta = (T_f - T_d)/T_d$. Note that the maximum value of δa is $2a$. The thermal relaxation time is

$$\tau_{\text{th}} = \frac{c_d \rho_d \delta a^2}{k_d}, \quad (28)$$

where c_d is the specific heat capacity of the particle.

Figure 7 shows the thermal relaxation time τ_{th} for $10 \mu\text{m} - 10 \text{cm}$ particles in the disk of model A. We set the particle bulk density $\rho_d = 1 \text{ g cm}^{-3}$, the specific heat capacity $c_d = 10^7 \text{ erg g}^{-1} \text{ K}^{-1}$, and the thermal conductivity $k_d = 10^2 \text{ erg s}^{-1} \text{ cm}^{-1} \text{ K}^{-1}$. The temperature difference Δ is calculated by equation (A17). At small distances from the star, radiative cooling $4\varepsilon\sigma_{\text{SB}}T_d^4$ dominates in determining Δ in equation (A17), and $\Delta \approx 1/4$. Thus, τ_{th} is independent of the particle size a , and is proportional to T_d^{-6} . In our model $T_d \propto r^{-1/2}$, and thus $\tau_{\text{th}} \propto r^3$. At large distances, on the other hand, internal

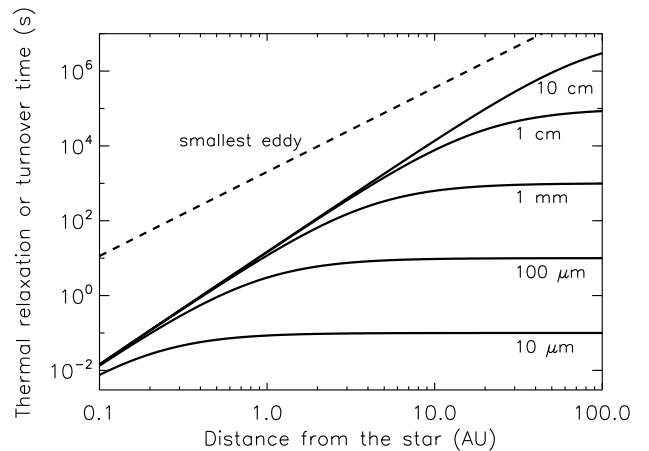


FIG. 7.— Thermal relaxation times of cylindrical particles of various sizes are plotted by the solid lines against the distance from the star. The dashed line shows the turnover time, τ_{ed} , of the smallest eddies for $\alpha_{\text{tur}} = 10^{-2}$.

thermal conduction $k_d T_d / a$ determines Δ . In this case, the skin depth is $\delta a = a$. Hence, τ_{th} is proportional to a^2 and independent of r .

If the rotation period of the particle is smaller than τ_{th} , photophoresis is considerably suppressed. Particle rotation can be excited by several mechanisms such as Brownian motion, gas turbulent motion, collisions with other dust particles, and the photophoretic force itself can induce rotation if it has an offset from the mass center. Detailed calculation of the rotation period for each mechanism is beyond the scope of this paper. Here, we make a rough estimate of the rotation speed induced by turbulence and by the photophoretic force.

Suppose that the gas disk has isotropic turbulence with the Kolmogorov energy spectrum. We assume that the largest eddies have size $L = \alpha_{\text{tur}}^{1/2} h_g$ and velocity $V = \alpha_{\text{tur}}^{1/2} c_s$, where α_{tur} is the “ α -viscosity” parameter (Cuzzi et al. 2001). The energy of turbulent motion cascades down to smaller eddies, and finally dissipates by the molecular viscosity. From dimensional analysis, the energy dissipation rate per unit mass is $\dot{\varepsilon} \sim V^3/L \sim \alpha_{\text{tur}} c_s^2 \Omega_K$. The eddy turnover time is faster for smaller eddies and that for the smallest eddies is

$$\tau_{\text{ed}} \sim \left(\frac{\eta_{\text{vis}}}{\rho_g \dot{\varepsilon}} \right)^{1/2} \sim \alpha_{\text{tur}}^{-1/2} \left(\frac{l}{h_g} \right)^{1/2} \Omega_K^{-1}, \quad (29)$$

where $\eta_{\text{vis}} = l v_T \rho_g / 2$ is the molecular viscosity (Weidenschilling 1984). The smallest eddies can induce a particle rotation period as short as τ_{ed} , if the particle is well coupled to the turbulent motion of the smallest eddies. However, if the particle does not strongly couple to the gas, the rotation period is longer than τ_{ed} . In Figure 7, the turnover time, τ_{ed} , of the smallest eddies is plotted by the dashed line for $\alpha_{\text{tur}} = 10^{-2}$. The particle rotation period induced by gas turbulence is expected to be larger than the dashed line, and therefore is much longer than the thermal relaxation time.

We next consider rotation induced by the torque exerted by photophoresis. Consider again a cylindrical dust particle and suppose that the photophoretic force is exerted on a point at a distance b from the cylinder axis.

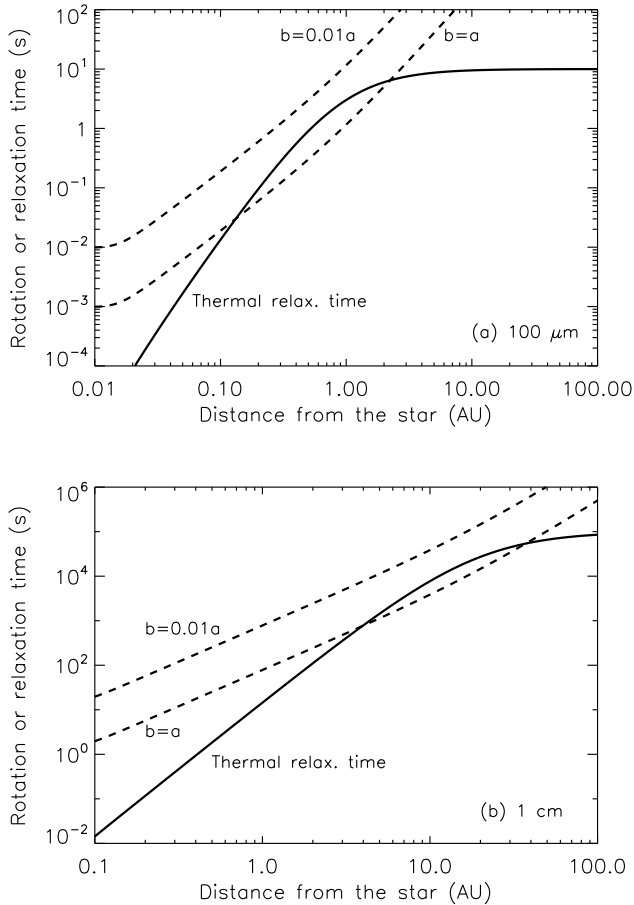


FIG. 8.— Times taken for a particle to rotate 180 degree by photophoresis are plotted by the dashed lines. The photophoretic force is exerted on a point at a distance $b = a$ or $b = 0.01a$ from the cylinder axis. The solid line shows the thermal relaxation time. (a) For $100 \mu\text{m}$ particles. (b) For 1 cm particles.

The torque is $K = bF_{\text{ph}}$. The value of b is unknown, and we treat b as a free parameter. The principal moment of inertia of the cylinder (for the axis perpendicular to the cylinder axis) is $I_{xx} = 7\pi a^5 \rho_d / 6$. The time needed for an initially stationary particle to rotate 180 degree is

$$\tau_{\text{rot}} = \left(\frac{2\pi I_{xx}}{K} \right)^{1/2} = \left(\frac{7\pi^2 \rho_d a^5}{3bF_{\text{ph}}} \right)^{1/2}. \quad (30)$$

In Figure 8, the rotation time τ_{rot} is plotted for assumed off-centers $b = a$ and $b = 0.01a$. If the photophoretic force has a large off-center ($b = a$), the rotation time can be shorter than the thermal relaxation time at $0.1 - 2$ AU for $100 \mu\text{m}$ particles and at $4 - 40$ AU for 1 cm particles. In such regions, photophoresis is probably significantly suppressed. In order for photophoresis to work effectively in the whole disk, the off-center of the photophoretic force has to be as small as $b = 0.01a$.

5.2. Characteristic Structure Due to Photophoresis

The dust disk structure that photophoresis makes has three zones: the outer disk, the inner disk, and the inner hole. The outer disk is composed of small ($a \lesssim 1 \text{ mm}$ or $\beta \gtrsim 0.01$) particles, and their dynamics is controlled mainly by radiation pressure. The inner disk is composed

of large ($a \gtrsim 100 \mu\text{m}$ or $\beta \lesssim 0.01$) particles accumulating there due to photophoresis. The boundary between the outer and inner regions is at $10 - 100$ AU, depending on the gas density profile. The inner hole opens inside ~ 0.1 AU, where the Knudsen number Kn is smaller than unity for particles that photophoresis effectively works on ($a = 100 \mu\text{m} - 10 \text{ cm}$).

The structure formed by photophoresis should be compared to the structure of gas-free disks. Modeling of gas-free dust disks also shows zonal structure that consists of the outer extended disk, the inner disk, and the inner hole (Thébault & Augereau 2005; Wyatt 2006; Strubbe & Chiang 2006; Krivov et al. 2006). In their models, a planetesimal belt is assumed and dust particles are continuously produced by planetesimal collisions. The inner disk is composed of large particles whose orbits are hardly affected by radiation pressure and are nearly circular. Thus, the location and width of the inner disk are basically similar to those of the planetesimal belt. Outside the planetesimal belt, the outer disk extends and it is composed of small particles whose β -value is large. Their orbits are strongly influenced by radiation pressure and are excited to highly eccentric orbits. In the model of Thébault & Augereau (2005), the particles of the outer disk have $\beta > 0.05$, which is relatively larger than β of our models. In our models, particles' β of the outer disk can be as small as 0.01. Therefore, infrared to millimeter radio observations of outer disks and determination of the particle size will provide key information for determining which model is plausible.

Our models of photophoresis also predict that an inner hole opens in the dust disk, but the gas still fills the hole. This is a significant feature, but it is difficult to test this with the present observational techniques. We have to observe the gas, but the amount of the gas of optically thin disks is probably quite small, and most of Vega-type stars do not have gas in an amount exceeding the current detection limit. Further, the radius of the inner hole is of the order of 0.1 AU, and the temperature there is close to the sublimation temperature of the dust. (The temperature exceeds 1500 K inside 0.03 AU of our model disks.) Therefore, we need a careful observation that can distinguish between the inner holes made by photophoresis and by dust sublimation.

5.3. Summary

Dust accumulation by photophoresis is studied. We use formulae of the photophoretic force that are applicable for the free molecular regime and for the slip-flow regime. The main results are as follows.

1. Particle accumulation occurs at a point where the outward acceleration on the gas by the pressure gradient equals to the outward acceleration on the particle by radiation pressure and photophoresis.

2. Photophoresis makes an inner disk composed of relatively large particles ($a = 100 \mu\text{m} - 10 \text{ cm}$). The inner disk extends between 0.1 AU and $10 - 100$ AU, surrounded by the outer disk composed of small particles ($a \lesssim 1 \text{ mm}$).

3. An inner hole opens inside ~ 0.1 AU. The inner hole radius is determined by the condition $\text{Kn} = 1$ for the maximum size particles that photophoresis effectively works on ($a = 100 \mu\text{m} - 10 \text{ cm}$).

Photophoresis works effectively only when the disk is

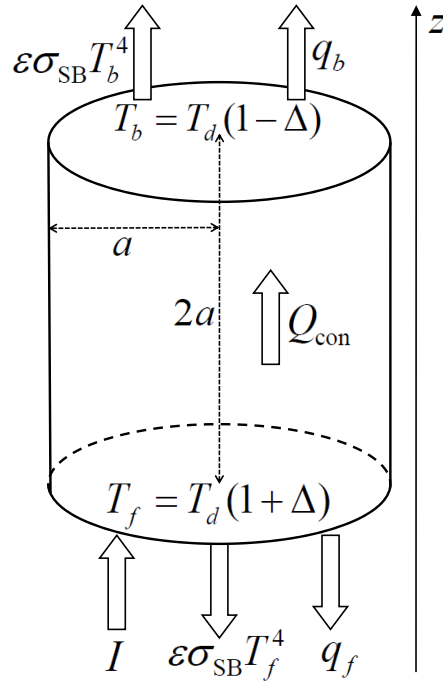


FIG. 9.— A cylindrical dust particle of radius a and height $2a$. Incident stellar flux I is parallel to the cylinder axis (z -axis) and irradiates the front surface. Radiation fluxes from the front and back surfaces are $\varepsilon\sigma_{\text{SB}}T_f^4$ and $\varepsilon\sigma_{\text{SB}}T_b^4$, respectively. The fluxes of heat conduction to the gas are q_f and q_b , and the heat flux inside the particle is Q_{con} .

optically thin. Most of small ($\lesssim 10 \mu\text{m}$) dust grains must be removed from the disk such that their column density to the star becomes smaller than $10^{-3} \text{ g cm}^{-2}$. For example, at 1 AU, the dust density must be smaller than $10^{-16} \text{ g cm}^{-3}$, i.e., 10^{-5} times smaller than the value of the minimum mass solar nebula model (Hayashi et al. 1985). The gas disk also must be optically thin. Figure 5 shows that the gas surface density must be smaller than $10^2 - 10^3 \text{ g cm}^{-2}$. At 0.1 AU, where the typical ray from the star enters the disk (for the dust particles at $r \gg 0.1 \text{ AU}$), this value is $\sim 10^{-2}$ times smaller than the value of the minimum mass solar nebula model (Hayashi et al. 1985). Even in such a tenuous gas disk, the photophoretic force is strong enough to change the dust disk structure inside a few AU, as shown by model A (Figure 2a). If the gas density is more tenuous than model A, the region where photophoresis has a substantial effect shrinks toward the central star. In a gas disk with 0.1 times smaller gas density than model A, photophoresis

on millimeter sized particles works effectively only inside 1 AU, and in a disk with 10^{-2} times smaller gas density, the effective region shrinks to 0.3 AU.

We thank Ingrid Mann, Tadashi Mukai, Yoichi Itoh, and Yoshitsugu Nakagawa for useful discussions. We are grateful to Takashi Tsuji for extensive and helpful discussions and for kindly providing his numerical code to calculate the gas opacity. We are grateful to anonymous referees for their constructive comments. This work was supported by the 21st Century COE Program, “The Origin and Evolution of Planetary Systems,” of the Ministry of Education, Culture, Sports, Science, and Technology (MEXT) of Japan, and also by the Grant-in-Aid for Scientific Research, No. 17740107 and No. 17039009, of the MEXT. OK is grateful to Gerhard Wurm and acknowledges the support of the Deutsche Forschungsgemeinschaft.

APPENDIX

A SIMPLE ESTIMATE OF THE PHOTOPHORETIC FORCE

In this Appendix, we estimate the magnitude of the photophoretic force using a simple calculation.

We consider a cylindrical dust particle with radius a and height $2a$ (see Figure 9). The particle is surrounded by the gas of temperature T_g . In general, T_g differs from the average temperature of the particle T_d . In deriving the photophoretic force below, we assume $T_g = T_d$, and consider $T_g \neq T_d$ cases later. The incident radiation flux, I , is parallel to the cylinder axis (z -axis) and irradiates the front surface. The temperature at the front surface increases to T_f and it radiates energy flux $\varepsilon\sigma_{\text{SB}}T_f^4$, where ε is the emissivity. Some of the incident energy is conducted to the gas with a rate q_f per unit area, and the residual energy flows to the back surface with a rate Q_{con} per unit area. For simplicity, we ignore the energy transfer through the side surface. The temperature of the back surface is T_b . The back surface radiates energy flux $\varepsilon\sigma_{\text{SB}}T_b^4$, and conducts heat to the gas with a rate q_b . In an equilibrium state, the

temperature inside the particle varies linearly along the cylinder axis, and thus its values at the front and back surfaces are written as

$$T_f = T_d(1 + \Delta) , \quad (\text{A1})$$

$$T_b = T_d(1 - \Delta) , \quad (\text{A2})$$

respectively. The energy balance reads

$$I - \varepsilon\sigma_{\text{SB}}T_f^4 - q_f = Q_{\text{con}} = \varepsilon\sigma_{\text{SB}}T_b^4 + q_b . \quad (\text{A3})$$

We calculate each term of equation (A3). First we consider free molecular photophoresis ($\text{Kn} \gg 1$). The radiative fluxes from the front and back surfaces are, assuming $\Delta \ll 1$,

$$\varepsilon\sigma_{\text{SB}}T_f^4 = \varepsilon\sigma_{\text{SB}}T_d^4(1 + 4\Delta) , \quad (\text{A4})$$

$$\varepsilon\sigma_{\text{SB}}T_b^4 = \varepsilon\sigma_{\text{SB}}T_d^4(1 - 4\Delta) , \quad (\text{A5})$$

respectively. The thermal conduction to the gas at the front surface is divided as

$$q_f = q_f^- - q_f^+ , \quad (\text{A6})$$

where q_f^- is the energy loss from the particle that is taken by the gas molecules ejected from the front surface, and q_f^+ is the energy gain that is given by the adsorbed molecules. In the free molecular approximation ($\text{Kn} \gg 1$), the velocity distribution of the adsorbed molecules is written as $\alpha f^+(\mathbf{v})$, where $0 \leq \alpha \leq 1$ is the accommodation coefficient, $f^+(\mathbf{v})$ is the Maxwellian velocity distribution of the temperature T_g and number density n_g ,

$$f^+(\mathbf{v}) = n_g \left(\frac{m_g}{2\pi k_B T_g} \right)^{3/2} \exp \left(-\frac{m_g |\mathbf{v}|^2}{2k_B T_g} \right) , \quad (\text{A7})$$

and m_g is the mass of a molecule. We define $f^+(\mathbf{v})$ to have non-zero values even for particles going away from the surface ($v_z > 0$). The energy gain is

$$q_f^+ = \alpha \int_{v_z < 0} \frac{1}{2} m_g v_z |\mathbf{v}|^2 f^+ d\mathbf{v} = \frac{1}{2} \alpha P v_T , \quad (\text{A8})$$

where v_z is the velocity component normal to the front surface, $P = \pi \rho_g v_T^2 / 8$ is the gas pressure, and $v_T = \sqrt{8k_B T_g / \pi m_g}$ is the mean thermal speed of gas molecules. The molecules ejected from the front surface are assumed to have a Maxwellian velocity distribution, $\alpha f^-(\mathbf{v})$, of the temperature T_f . The energy loss is

$$q_f^- = \alpha \int_{v_z > 0} \frac{1}{2} m_g v_z |\mathbf{v}|^2 f^- d\mathbf{v} = \frac{\pi}{16} \alpha \rho_f^- (v_f^-)^3 , \quad (\text{A9})$$

where $v_f^- = \sqrt{8k_B T_f / \pi m_g}$ and the ‘‘density’’ of ejected molecules (for $\alpha = 1$) is

$$\rho_f^- = \int_{\text{all } \mathbf{v}} m_g f^- d\mathbf{v} . \quad (\text{A10})$$

From mass conservation between the adsorbed and ejected molecules ($\alpha \rho_f^- v_f^- = \alpha \rho_g v_T$),

$$\rho_f^- = \left(\frac{T_g}{T_f} \right)^{1/2} \rho_g . \quad (\text{A11})$$

Then, we obtain

$$q_f^- = \frac{\alpha P v_T T_f}{2 T_g} . \quad (\text{A12})$$

If the gas temperature and the average dust temperature are same ($T_g = T_d$), the thermal conduction to the gas is

$$q_f = \frac{1}{2} \alpha P v_T \Delta . \quad (\text{A13})$$

Similarly, the thermal conduction to the gas from the back surface is

$$q_b = -\frac{1}{2} \alpha P v_T \Delta . \quad (\text{A14})$$

The thermal conduction inside the particle is

$$Q_{\text{con}} = k_d \frac{T_d \Delta}{a} . \quad (\text{A15})$$

Collecting all the above expressions of the terms in equation (A3), the particle temperature is solved as

$$T_d = \left(\frac{I}{2\varepsilon\sigma_{\text{SB}}} \right)^{1/4}, \quad (\text{A16})$$

and

$$\Delta = \frac{I}{2[k_d T_d/a + 4\varepsilon\sigma_{\text{SB}}T_d^4 + \alpha P v_T/2]}. \quad (\text{A17})$$

The force exerted on the front surface by the ejected molecules is

$$F_f = \pi a^2 \alpha \int_{v_z > 0} m_g v_z^2 f^- d\mathbf{v} = \frac{\pi a^2 \alpha P}{2} \left(\frac{T_f}{T_g} \right)^{1/2}, \quad (\text{A18})$$

and on the back surface,

$$F_b = \frac{\pi a^2 \alpha P}{2} \left(\frac{T_b}{T_g} \right)^{1/2}. \quad (\text{A19})$$

Assuming $T_g = T_d$ and $\Delta \ll 1$, the photophoretic force is

$$F_{\text{ph},f} = F_f - F_b = \frac{\pi a^2 \alpha I P}{4[k_d T_d/a + 4\varepsilon\sigma_{\text{SB}}T_d^4 + \alpha P v_T/2]}, \quad (\text{A20})$$

which can be compared to equation (3) for the spherical particle case.

We consider how the photophoretic force changes from equation (A20) when the dust temperature T_d differs from the gas temperature T_g . For simplicity, we consider the cases where the thermal conduction to the gas can be neglected. With $q_f = q_b = 0$ in equation (A3), the photophoretic force becomes

$$F_{\text{ph},f} = \frac{\pi a^2 \alpha I P}{4[k_d T_d/a + 4\varepsilon\sigma_{\text{SB}}T_d^4]} \left(\frac{T_d}{T_g} \right)^{1/2}, \quad (\text{A21})$$

which differs from the $T_d = T_g$ case by a factor $(T_d/T_g)^{1/2}$. We consider further the cases where the temperature variation inside the dust particle is large ($\Delta \sim 1$). Such a situation arises if $\varepsilon\sigma_{\text{SB}}T_d^4 \gg k_d T_d/a$, $\alpha P v_T$. In this case, $T_f = (I/\varepsilon\sigma_{\text{SB}})^{1/4}$ and $T_b=0$, and thus the photophoretic force is $F_{\text{ph},f} = F_f = \pi a^2 \alpha P (T_f/T_g)^{1/2}/2$. The photophoretic force calculated by equation (A21), which assumes $\Delta \ll 1$, reduces to $F_{\text{ph},f} = F_f/(4 \cdot 2^{1/8})$, when the term $k_d T_d/a$ is neglected. Thus, in the extreme case where $\Delta \sim 1$, equation (A21) underestimates the photophoretic force by a factor $4 \cdot 2^{1/8}$.

In the slip-flow regime ($\text{Kn} \ll 1$), thermal conduction to the gas is estimated as $q_f \sim q_b \sim k_g T_d \Delta/a$, where k_g is the thermal conductivity of the gas. The temperature difference is

$$\Delta \sim \frac{I}{[(k_d + k_g)T_d/a + 4\varepsilon\sigma_{\text{SB}}T_d^4]}. \quad (\text{A22})$$

Because of the temperature variation along the dust surface, a slip flow of the gas arises. The velocity of the thermal slip is

$$v_s \sim C_s v_T \Delta \text{Kn}, \quad (\text{A23})$$

where $C_s \sim 1$ is the thermal slip coefficient (Lifshitz & Pitaevskii 1981). The particle, which moves in the gas with a velocity v_s , experiences Stokes gas drag,

$$F_{\text{Stokes}} \sim a \eta_{\text{vis}} v_s \quad (\text{A24})$$

where $\eta_{\text{vis}} = l v_T \rho_g / 2 = v_T m_g / (2\sqrt{2}\sigma_{\text{mol}})$ is the molecular viscosity. ($F_{\text{Stokes}} = 6\pi a \eta_{\text{vis}} v_s$ if the particle is spherical.) In the equilibrium state, the photophoretic force balances with the Stokes drag force, and is estimated as

$$F_{\text{ph},s} \sim \frac{C_s a^2 k_B I}{\sigma_{\text{mol}} k_d} \left(1 + \frac{4a\varepsilon\sigma_{\text{SB}}T_d^3}{k_d} + \frac{k_g}{k_d} \right)^{-1} \text{Kn}, \quad (\text{A25})$$

which can be compared to equation (5). In the above derivation, we neglect the temperature jump at the surface and the velocity slip due to imperfect sticking of the gas to the surface ($C_t = C_m = 0$).

SLIP-FLOW REGIME PHOTOPHORESIS

In this Appendix, we derive the expression for the photophoretic force in the slip-flow regime, equation (5), taking into account the radiative cooling of the particle. We follow the derivation described in Mackowski (1989). (The assumption is as follows. The mean temperatures of the gas and the dust, T_g and T_d , are the same. The temperature variation from the mean value is small. The Reynolds number is much less than unity and thus gas drag obeys the

Stokes law. The gas temperature is determined only by the heat conduction from the dust and inside the gas.) Here, we do not rewrite Mackowski's derivation again, but we describe what is modified when radiative cooling is taken into account. In this Appendix, the numbering of equations with "M" means that they refer to equations of Mackowski (1989). For the meaning of the symbols see Mackowski (1989). However, for some variables, we have used different symbols in the main text, and we keep the same notation in the Appendix. When we use a different symbol from Mackowski (1989), the corresponding symbol in Mackowski (1989) is given in brackets.

The basic equations (M11)-(M14) and the boundary conditions (M15)-(M20) are not changed except that equation (M16) is modified as

$$-k_g \frac{\partial \hat{T}_g}{\partial r} + \varepsilon \sigma_{\text{SB}} \hat{T}_d^4 = -k_d \frac{\partial \hat{T}_d}{\partial r}, \quad (\text{B1})$$

where $\hat{T}_d(T_s)$ is the temperature inside the dust particle, $\hat{T}_g(T_g)$ is the gas temperature, and $k_d(k_s)$ is the thermal conductivity of the dust. Then, equation (M22) becomes

$$D_n = \frac{nG_n(1) - G'_n(1)}{(4\varepsilon\sigma_{\text{SB}}T_d^3 a/k_d + n)[1 + (n+1)C_t l/a] + (n+1)k_g/k_d}, \quad (\text{B2})$$

where $T_d(T_0)$ is the mean temperature of the dust, $C_t(c_t)$ is the coefficient of the jump condition, and we correct the typo in the sign of the original equation. Equation (M28) is not modified when it is expressed using D_1 as

$$c_1 = \frac{3(1 + 2C_m l/a)}{4(1 + 3C_m l/a)} - \frac{C_s \eta_{\text{vis}} D_1}{2V_0 \rho_g a(1 + 3C_m l/a)}, \quad (\text{B3})$$

where $\eta_{\text{vis}}(\eta)$ is the molecular viscosity, and $C_m(c_m)$ and $C_s(c_s)$ are the coefficients of the jump conditions. Finally equation (M29) becomes

$$F_p = -\frac{4\pi C_s \eta_{\text{vis}}^2 a I J_1}{k_d T_d \rho_g} \frac{1}{(1 + 3C_m l/a)[(4\varepsilon\sigma_{\text{SB}}T_d^3 a/k_d + 1)(1 + 2C_t l/a) + 2k_g/k_d]}, \quad (\text{B4})$$

where $I(I_\lambda)$ is the incident flux of the starlight. Substitution of the expression for $\eta_{\text{vis}}^2 = \sqrt{2} l \rho_g k_B T_d / (\pi \sigma_{\text{mol}})$ and taking the absolute value give equation (5).

REFERENCES

- Alexander, R. D., Clarke, C. J., & Pringle, J. E. 2006, MNRAS, 369, 216
 Alexander, R. D., Clarke, C. J., & Pringle, J. E. 2006, MNRAS, 369, 229
 Alexander, D. R., & Ferguson, J. W. 1994, ApJ, 437, 879
 Ardila, D. R., et al. 2005, ApJ, 627, 986
 Augereau, J. C., Lagrange, A. M., Mouillet, D., & Ménard, P. A. 1999a, A&A, 350, L51
 Beresnev, S., Chernyak, V., & Fomyagin, G. 1993, Phys. Fluids A, 5, 2043
 Borysow, A., Jorgensen, U. G., & Zheng, C. 1997, A&A, 324, 185
 Bottke, W. F., Jr., Vokrouhlický, D., Rubincam, D. P., & Broz, M., in Asteroids III, ed. W. F. Bottke Jr., A. Cellino, P. Paolicchi, & R. P. Binzel, (Tucson: University of Arizona Press), 395
 Brownlee, D., et al. 2006, Science, 314, 1711
 Burns, J. A., Lamy, P. L. & Soter, S. 1979, Icarus, 40, 1
 Chapman, S., & Cowling T. G. 1970, The Mathematical Theory of Non-Uniform Gases (Cambridge: Cambridge University Press)
 Chen, C. H., & Kamp, I. 2004, ApJ, 602, 985
 Clampin, M., et al. 2003, AJ, 126, 385
 Clarke, C. J., Gendrin, A., & Sotomayor, M. 2001, MNRAS, 328, 485
 Coulson, I. M., Dent, W. R. F., & Greaves, J. S. 2004, MNRAS, 348, L39
 Cuzzi, J. N., Hogan, R. C., Paque, J. M., & Dobrovolskis, A. R. 2001, ApJ, 546, 496
 Dent, W. R. F., Greaves, J. S., & Coulson, I. M. 2005, MNRAS, 359, 663
 Dullemond, C. P., & Dominik, C. 2005, A&A, 434, 971
 Ferguson, J. W., Alexander, D. R., Allard, F., Barman, T., Bodnarik, J. G., Hauschildt, P. H., Heffner-Wong, A., & Tamanai, A. 2005, ApJ, 623, 585
 Fisher, R. S., Telesco, C. M., Piña, R. K., Knacke, R. F., & Wyatt, M. C. 2000, ApJ, 532, L141
 Goto, M., Usuda, T., Dullemond, C. P., Henning, Th., Linz, H., Stecklum, B., & Suto, H. 2006, ApJ, 652, 758
 Greaves, J. S. 2004, MNRAS, 351, L99
 Greaves, J. S., Mannings, V., & Holland, W. S. 2000, Icarus, 143, 155
 Hartmann, L., Calvet, N., Gullbring, E., & D'Alessio, P. 1998, ApJ, 495, 385
 Hayashi, C., Nakazawa, K., & Nakagawa, Y. 1985, in Protostars and Planets II, ed. D. C. Black & M. S. Matthews (Tucson: Univ. of Arizona Press), 1100
 Hidy, G. M., & Brock, J. R. 1967, J. Geophys. Res., 72, 455
 Hollenbach, D., Johnstone, D., Lizano, S., & Shu, F. H. 1994, ApJ, 428, 654
 Krauss, O., & Wurm, G. 2005, ApJ, 630, 1088
 Krauss, O., Wurm, G., Mousis, O., Petit, J. -M., Horner, J., & Alibert, Y. 2007, A&A, 462, 977
 Krivov, A. V., Löhne, T., & Sremcevic, M. 2006, A&A, 455, 509
 Lifshitz, E. M., & Pitaevskii, L. P. 1981, Physical Kinetics (Oxford: Butterworth-Heinemann)
 Liseau, R., & Artymowicz, P. 1998, A&A, 334, 935
 Mackowski, D. W. 1989, Int. J. Heat Mass Transfer, 32, 843
 Marsh, K. A., Silverstone, M. D., Becklin, E. E., Koerner, D. W., Werner, M. W., Weinberger, A. J., & Ressler, M. E. 2002, ApJ, 573, 425
 Miyake, K., & Nakagawa, Y. 1993, Icarus, 106, 20
 Mouillet, D., Lagrange, A. M., Augereau, J. C., & Menard, F. 2001, A&A, 372, L61
 Mousis, O., Petit, J.-M., Wurm, G., Krauss, O., Alibert, Y., & Horner, J. 2007, A&A, 466, L9
 Nakagawa, Y., Sekiya, M., & Hayashi, C. 1986, Icarus, 67, 375
 Nomura, H., & Nakagawa, Y. 2006, ApJ, 640, 1099
 Petit, J.-M., Mousis, O., Alibert, Y., & Horner, J. 2006, Lunar Planet. Sci., 37, 1558
 Presley, M. A., & Christensen, P. R. 1997, J. Geophys. Res. E, 102, 6535
 Strubbe, L. E., & Chiang, E. I. 2006, ApJ, 648, 652
 Takeuchi, T., & Artymowicz, P. 2001, ApJ, 557, 990

- Takeuchi, T., Clarke, C. J., & Lin, D. N. C. 2005, *ApJ*, 627, 286
Tanaka, H., Himeno, Y., & Ida, S. 2005, *ApJ*, 625, 414
Thébaud, P., & Augereau, J.-C. 2005, *A&A*, 437, 141
Tsuji, T. 1966, *PASJ*, 18, 127
Tsuji, T. 1971, *PASJ*, 23, 553
Tsuji, T. 2002, *ApJ*, 575, 264
Weidenschilling, S. J. 1984, *Icarus*, 60, 553
Weidenschilling, S. J., & Cuzzi, J. N. 1993, in *Protostars and Planets III*, ed. E. H. Levy & J. I. Lunine (Tucson:Univ. of Arizona Press), 1031
Weinberger, A. J., Becklin, E. E., Schneider, G., Smith, B. A., Lowrance, P. J., Silverstone, M. D., Zuckerman, B., & Terrile, R. J. 1999, *ApJ*, 525, L53
Weinberger, A. J., Rich, R. M., Becklin, E. E., Zuckerman, B., & Matthews, K. 2000, *ApJ*, 544, 937
Wurm, G., & Krauss, O. 2006, *Icarus*, 180, 487
Wyatt, M. C. 2006, *ApJ*, 639, 1153
Zuckerman, B., Forveille, T., & Kastner, J. H. 1995, *Nature*, 373, 494